Evaluation of non-uniform tyre contact stresses on thin asphalt pavements

M De Beer, C Fisher

CSIR Transportek, PO Box 395, Pretoria 0001, South Africa, e-mail: mbeer@csir.co.za

F J Jooste

Director: Pavement Analysis Systems cc. PO Box 634. La Montagne 0184, e-mail: fritzj@icon.co.za

ABSTRACT: Improved quantification of the shape and distribution of actual tyre-pavement contact stresses resulted in enhanced definitions of 3D-tyre-pavement contact stresses for the design and analysis of flexible pavements. It is now possible to describe the 3D-load/stress regimes with a series of discrete load values that were measured using Stress-In-Motion (SIM) technology, as well as being predicted from trained Artificial Neural Networks (ANNs). This paper illustrates the importance of these new load/stress inputs in pavement design on pavements with relatively thin asphalt surfacings, typically used in southern Africa. This investigation concentrates on the quantification of several pavement response parameters as a result of non–uniform and non-circular shaped contact stresses at different asphalt moduli, compared to the traditional circular uniformly loaded tyre patch. The Finite Element Method (FEM) was used for the detailed analyses. In addition, the responses of an *un-cracked* and *cracked* pavement structure were also compared, under circular and rectangular loading shapes of varying levels of loads and contact stresses using a customised semi-analytical FEM code. The response data were benchmarked with multi-layered linear elastic theory, and also indicated the importance of both the load shape and level of contact stress on pavement performance. The importance of using and managing actual tyre-pavement contact stress data for more rational design and analysis of pavements incorporating thin asphalt layers is highlighted.

1. INTRODUCTION AND BACKGROUND

Evaluation of road surface distress in South Africa has shown that there is little commonality among observed distresses, pavement loading and the material properties considered in pavement design, performance and asphalt mix design [De Beer et al, 1999]. Efforts to address the foregoing engineering problem (i.e. bridge the gap) were reported at the last ISAP conference [ISAP, 1997]. It was shown that improvements in measuring technology of the tyre-pavement contact stress regimes have resulted in an enhanced definition of three- dimensional (3D) tyre-pavement contact stress description for pavement design and analysis [De Beer et al, 1997, 1999; Woodside, 1992; Woodside et al, 1992, 1999; Roque et al, 1998; Himeno et al, 1997]. It is now possible to describe the load/stress regime with a series of discrete load values that were measured directly using Stress- In-Motion (SIM) technology, or predicted from trained artificial neural networks (ANNs) [El-Gindy et al, 1999].

The purpose of this paper is to illustrate the value and use of the non-circular and non-uniform 3D-load/stress inputs in pavement design and analysis on pavements with relatively thin asphalt concrete layers such as those typically used in southern Africa. The investigations were done, using Finite Element Methods (FEM). The first FEM investigation concentrated on the pavement response parameters as a result of the non–uniform and non-circular contact stress applications. The stress-strain responses of the asphalt layer in the area under and close to the tyre are investigated. The response data are compared with the standard uniform and circular loading case normally used for mechanistic pavement design and analysis in South Africa [Theyse et al, 1999].

The second semi-analytical FEM analysis was done using a rectangular load and contact stress, including a non-linear stress-stiffening model for the granular base. The analysis was done on a pavement with and without cracks in the bound layers (i.e. old asphalt and cementitious subbase). Both FEMs were "benchmarked" with the well-known multi-layered linear elastic theory. Amongst others, the investigation concentrated on the absolute maxima values and their location of certain pavement response parameters. In the first analysis these included vertical elastic strain, compressive stress, first invariant of stress, second invariant of strain and the maximum yield values against shear failure. The second FEM analysis included the effects of variable load and contact stress as they influenced the octahedral shear stress and strain energy of distortion, computed for the new thin asphalt-surfacing layer. The importance of using actual 3D-tyre-pavement contact stresses for the design and analysis of pavements incorporating thin asphalt layers is demonstrated. This also includes the relative importance of 3D-contact stresses

(including applied shear stresses) on the surface of the pavement, as opposed to use of the traditional 1D-vertical loading, without shear. The importance of including non-uniform tyre contact stresses as well as the addition of shear stress was also highlighted in other recent studies [Myers et al, 1999; Woodside et al, 1999; Douglas et al, 2001; Drakos et al, 2001; Himeno and Ikeda, 1997; Groenedijk et al, 1997; Weissman, 1999; Harvey and Blab, 2000; Long, 2001].

2. THIN LAYERED ASPHALT PAVEMENTS IN SOUTH AFRICA

According to the South African Bitumen and Tar Association (SABITA), the asphalt industry in southern Africa has seen an increase in the use of asphalt layers with thicknesses of between 20 mm and 30 mm. Here, ultra-thin layers are defined as those with a thickness of 25 mm or less. These layers have been used with success in Europe and are exclusively used to obtain desired functional properties (particularly riding quality, noise reduction and skid resistance) [Brosseaud, 1999]. Traditionally, the use of relatively thin (< 50 mm) flexible asphalt surfacings was, and still is, a popular method of providing a good all-weather surfacing for flexible pavements with granular or lightly cemented bases in southern Africa [HMA, 1998, 2000, 2001]. However, traditionally, relatively thick asphalt base pavements were typically constructed in the wetter regions of the country, such as the eastern part of KwaZulu-Natal. In these cases a typical design includes a 90 to 120 mm continuously graded asphalt base layers with a thin (40 mm) semi-gap-graded flexible asphalt surfacing. It is interesting to note here that, over the last few years, the use of a high quality granular base (G1) [TRH 14, 1985] has become more popular in this region. It has proved to be a more economic option, provided that the design and construction comply with the relatively strict construction standards specified for these unbound crushed stone base pavements. In almost all typical medium to heavy pavement structures the use of one or two 150 mm lightly cementitious (i.e. stabilized) subbase layers is compulsory in southern Africa. This is to provide a stable and solid platform for the construction of the various granular, cementitious or asphalt base layers (See also [TRH 4, 1996]), and therefore provides for a state of compression (stresses and strains in compression) within the stress-stiffening granular layer.

Approximately 17.2 per cent of the total actual road networks in South Africa, from provincial level upwards, are paved [De Beer et al, 1999]. There is, thus, a very large potential for mainly flexible asphalt surfacings in this country. Of the paved roads in South Africa, approximately 91 per cent incorporate a relatively thin (<50 mm) flexible asphalt surfacing or seal coat. Thirteen per cent of these pavements incorporate asphalt base layers of thicknesses varying approximately from 80 mm to 120 mm. In total, the asset value of Hot-Mix Asphalt (HMA) placed on National Roads in South Africa is approximately US$ 670 million[1]. As South Africa has to import crude oil at ever-increasing cost, with corresponding increases in the cost of bitumen, more cost - effective road construction, maintenance and rehabilitation is necessary and may be achieved with *improved* HMA design procedures and construction processes. It is believed that, amongst others, improved tyre-pavement contact stress models could play a central role in the more *rational* pavement design methodology, and therefore, also in the associated and more appropriate material testing for HMA.

3. APPROACH AND METHODOLOGIES APPLIED IN THIS STUDY

The approach used in this study is as follows:
- Study of an example of representative dynamic tyre loads on a typical South African road of average roughness;
- Transformation of these tyre loads to non-circular and non-uniform 3D-contact stresses experienced by pavements;
- Evaluation and presentation of latest contact stress information and its management in South Africa, based on the Stress-In-Motion (SIM) technology;
- Detailed pavement modelling, using two Finite Element Methods (FEM), i.e.:
  - NASTRAN code [NASTRAN, 2001], on a typical *new* pavement incorporating a thin asphalt surfacing using different measured tyre loadings compared to circular loading. The analysis was done using linear elastic material modelling, with Mohr-Coulomb failure criteria for the thin asphalt surfacing, and

---

[1] In South Africa, the average HMA cost = US$ 40/ton. On average HMA = 2400 kg/m³. Approximately16.8 million tons of HMA have been placed on National Roads in South Africa.

- A customised semi-analytical FEM model [Jooste, 2001], using non-linear material modelling for granular base and cracking in the bound layers to *study the effects of load shape and variable contact stresses* on a typical pavement during rehabilitation design; and

• Discussion, conclusions, and recommendations.

3.1. Study of an example of representative dynamic tyre loads on a typical South African road of average roughness

Since pavement loading from moving truck tyres is dynamic in nature, it is important to quantify this dynamic variation of the tyre load accurately for pavement design purposes. In a recent study by Steyn [Steyn, 2001], it was shown that, in South Africa, the tyre loading of a typical 7-axle interlink (1:2:2:2 configuration)[2] may vary by more than 20 per cent on a road with a roughness (HRI)[3] of 3.1 m/km. Figure 1 illustrates the left and right road pavement profiles, which vary between –0.15 m below and 0.2 m above the average profile. Figure 2 illustrates the calculated tyre loads of the left tyre on the steering axle, as well as the right outer tyre of the first leader axle of this truck, using the Dynamic Analysis and Design System (DADS) software code [DADS, 2000]. To indicate the typical variation in tyre loading resulted from this truck, the axles with minimum and maximum loading were selected. The tyres on the steering axle produced the highest average loading at 37 000 Newtons (N), while the first leading axle produced the lowest tyre loading, with an average of 17 500 N. Figure 2 indicates that the dynamic tyre load of the steering axle varied between approximately 24 700 N and 47 000 N, and that on the leading axle right-outer tyre (minimum on truck) varied between 12 400 N and 23 500 N. As indicated earlier, these tyre loadings were derived from dynamic analysis with the DADS computer code [Steyn, 1999], at the truck speed of 100 km/h. The truck was overloaded at 110 per cent (i.e. 10 per cent overload), on a road with an average roughness of HRI = 3.1 m/km.

In order to incorporate these loading effects in pavement design, the authors are convinced that the dynamic loading should be transformed either to estimated or directly measured 3D-tyre- pavement contact stresses. The computed tyre loads were converted to pavement contact stress, as shown in Figure 3 and Figure 4, using empirical algorithms developed and described by De Beer et al [1997][4]. Figure 3 indicates that the maximum dynamic vertical contact stress of the steering tyre varied between 1 380 kPa, and 1 591 kPa, with an average of approximately 1 500 kPa. For the leading axle, the maximum vertical contact stress varied between 1 260 kPa and 1368 kPa, with an average of 1 310 kPa. The derived dynamic lateral and longitudinal stresses under the tyre contact patch are shown in Figure 4. The variations of these stresses for the two tyres studied are summarised in Table 1.

Table 1. Variation in maximum contact stresses of the two tyres

Tyre	Condition	Max.Vertical Stresses (kPa)	Max. Transverse Stresses across tyre patch (kPa)	Max. Longitudinal Stresses along tyre patch (kPa)
Steering tyre-Left	Maximum	1 591	351	252
	Average	1 497	219	209
	Minimum	1 380	292	154
Right-outer tyre	Maximum	1 368	211	149
- First leading axle	Average	1 310	175	122
	Minimum	1 260	146	100

From the data in Table 1 it is clear that the vertical stress is the highest of the three stress components, followed by the transverse (or lateral) and the longitudinal stresses. The average stress ratio[5] is approximately 10:1.5:1. It is, however, important to note that these stress algorithms were based on SIM measurements done on free-rolling tyres, with no shear (i.e. steering angle = 0) [De Beer et al, 1999]. Figure 5 illustrates the histogram of the dynamic load obtained for the steering tyre, showing an approximate Gaussian distribution. Figure 6 contains the histograms

---

[2] 1:2:2:2 configuration indicated here incorporates one steering axle, and three sets of dual-tyred tandem axles, totalling seven (7) axles. The truck used for the study was a Mercedes Benz 2535S/32 truck tractor and Tandem-tandem Semi-Trailer. [3] HRI = Half-car Roughness Index [ISO, 1995]. [4] See Table 5, pp 207, in De Beer et al [1997], Tyre Type reference II: 11.00 X 20 14 ply, bias/cross ply rating.

[5] Stress Ratio = ratio between Vertical: Lateral: Longitudinal stress, with vertical stress set at a value of 10.

of the derived dynamic vertical, lateral and longitudinal contact stresses are given. The results show an approximate double Gaussian distribution for the lower stresses, i.e. transverse and longitudinal (154 MPa to 351 MPa), and an approximate Gaussian distribution for the maximum vertical stresses (1 380 MPa to 1 591 MPa). From a pavement design point of view, it is clear from these stress distributions that the pavement and its surface should therefore be able to accommodate these stresses on the pavement system (i.e. stress demand on the pavement surface). The pavement system should therefore be designed to carry these stresses over its design period, which ranges typically between 20 and 30 years, without premature failure. It is accepted that normal preventative maintenance will be carried out on the surface of the pavement, in order to assist with the current problem experienced with the functional and structural performance of road pavement surfaces in South Africa today, under increased tyre loads and stresses.

3.2. Tyre contact stress information and its management in South Africa

The research discussed in this paper relies heavily on previous basic work that was done on tyrepavement contact stresses, discussed elsewhere [De Beer, et al, 1997, 1998a, 1998b, 1999; Jooste and Lourens, 1998]. In summary, the Stress-In-Motion (SIM) technology was developed, using the Vehicle-Road Surface Pressure Transducer Array (VRSPTA) developed during the late 1990's in South Africa. The SIM Mark III device discussed in De Beer [1998a, b] and De Beer et al [1999], is a custom-designed VRSPTA system that measures the 3D-tyre-pavement contact stresses of all the tyres of slow moving (5 km/h) trucks. In South Africa the SIM device is typically installed at a weighbridge station with static scales [De Beer, 1998]. The system produced relatively large data files, and it is difficult to manage this data using normal spreadsheets. A custom-designed SIM data organizer was therefore developed to take care of these large data files. Some of the characteristics of the SIM data organiser are summarised in the next section.
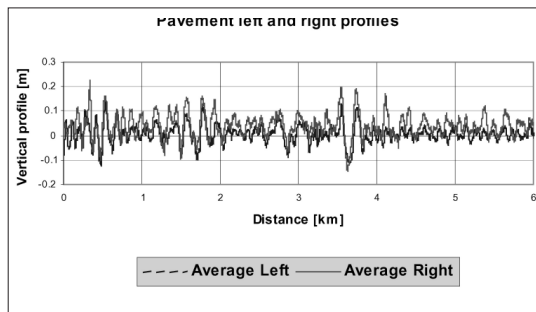

Figure 1
Road profiles used for the analysis:
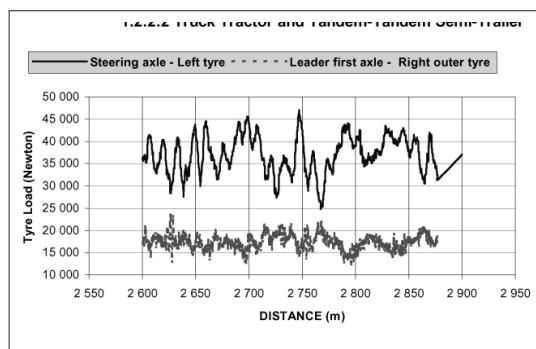Left and right track

Figure 2
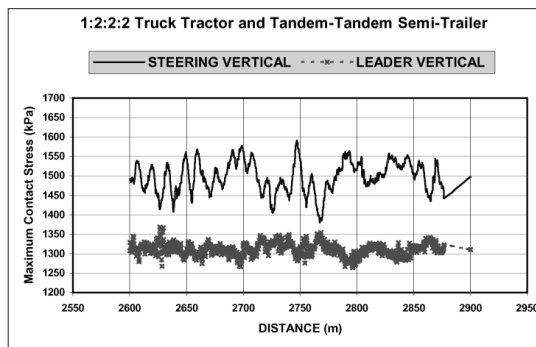Dynamic Load variation of
the steering and the leader tyres

Figure 3
Derived dynamic vertical contact
stresses along the pavement

Figure 4
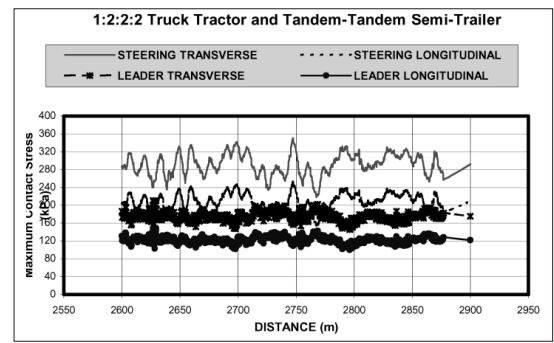Derived dynamic transverse (lateral)
and longitudinal contact stresses

Figure 5
Load frequency distribution of
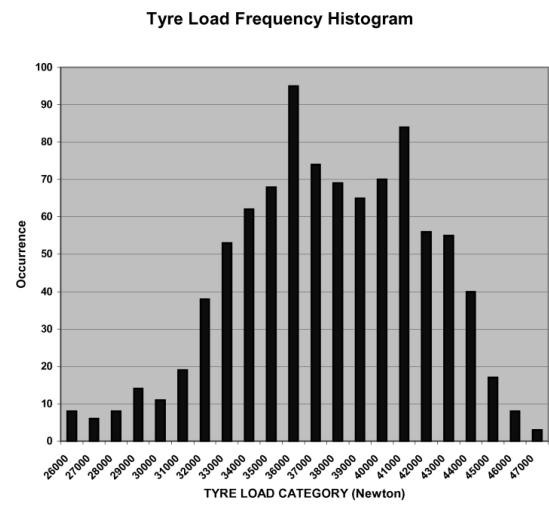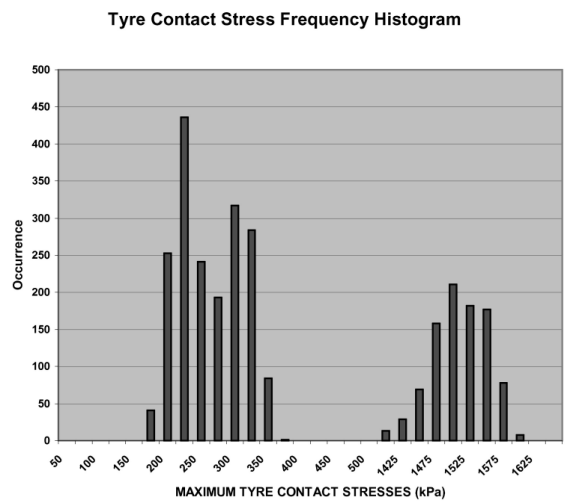the tyre loading for the left tyre on the
steering axle.

Figure 6
Contact Stress distribution of
the left tyre on the steering axle. Note:
Lower range for lateral and
longitudinal stresses, and upper range for
vertical stress.

3.2.1 Tyre Contact Stress-In-Motion (SIM) Data Organiser™

The Stress-In-Motion (SIM) measuring device uses an array of 84 transducers and is capable of taking measurements in 3 directions at a rate of over 1000 readings per second. This large quantity of data requires careful organisation if it is to be useful for later analysis and study. A SIM data organiser was developed on a multi-user multi-computer platform using an object-oriented database management system [Ringwood, 2001]. Figure 7 illustrates how the data is organised in a simple tree type catalogue of tests. In Figure 8, an example plot is given of the "footprints" of the vertical measured contact stress of all the tyres of a five-axle truck with a 1:1:1:1:1 configuration, with tandem axles and dual tyres. It is interesting to note that the maximum vertical loading was obtained under the two tyres on the steering axle, indicating tyre (and axle) loads approximately 30 per cent *higher* than for the other trailing axles. This corresponds also to the results of the DADS analysis discussed earlier. The implications of this need to be evaluated in terms of applied contact stresses from the tyres of the steering axles, compared with those of the trailing axles. This, however, is outside the scope of this paper.

3.3. Prediction of contact stresses using Artificial Neural Networks (ANNs)

The first neural network tyre contact stress prediction models were developed in 1998/9 by El-Gindy et al [1998, 1999], based on SIM tyre-pavement contact stress data sets that were measured for the Californian Highway Department (Caltrans) at the University of California at Berkeley (UCB) [De Beer et al, 1997]. The idea is that, because of the relatively expensive nature of actual tyre contact stress measurements, Artificial Neural Networks (ANN) could be trained on existing measured data sets. In this way cases of load or stress (which are not measured) could be predicted, based on known measurements. In a pilot study by El-Gindy et al [1998, 1999] the success of this method was illustrated for the prediction of vertical stress only. An example of the accuracy of this method is illustrated in Figures 9, 10 and 11, for a measured load of 26 kN and an inflation pressure of 620 kPa. Figure 9 the actual measured case, Figure 10 illustrates the ANN predicted case, and Figure 17 the prediction error surface, calculated as the difference between the measured and predicted cases above.

3.4. Detailed pavement modelling, using Finite Element Methods (FEM)

3.4.1 Introduction

In order to enable the effects of non-uniform and non-circular tyre-pavement contact stresses on pavement incorporating thin asphalt layers to be studied, detailed pavement analyses were done with the aid of two finite element method (FEM) software codes. In the first case, the commercial NASTRAN code was used for a 3D-model of the pavement. In this case the pavement was modelled as a new thinly surfaced pavement with the measured 3D-SIM loading data applied to the pavement, in contrast to the case where the load is modelled based on the assumption of a uniform circular stress. In the second case, an old pavement with an uncracked and cracked thin asphalt surfacing was modelled and analysed for distress potential, using a customised semi-analytical FEM [Jooste, 2001], to study the *effect of load and contact stress levels* on pavement response. The approaches for these analyses and results are discussed in the next two sections.

Figure 7

Typical perspective view of the vertical contact stress of an overloaded/under inflated tyre form an actual truck. Note the peak stresses at the tyre edges.
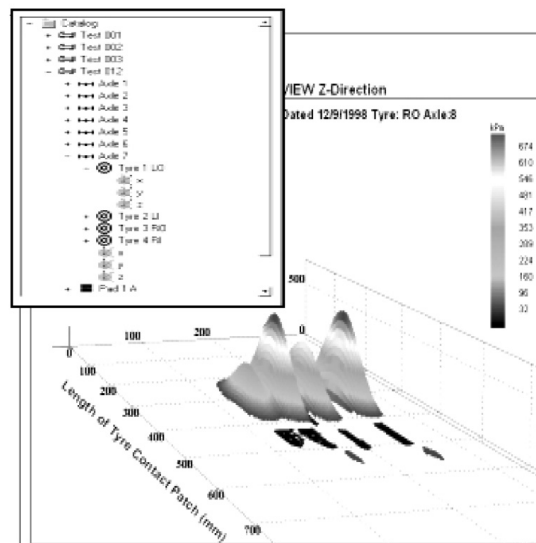
Tree-like layout of tests given in the subplot.

Figure 8

Typical vertical contact stress contours of all the tyres of typical a five axle truck measured with the SIM Mk III system
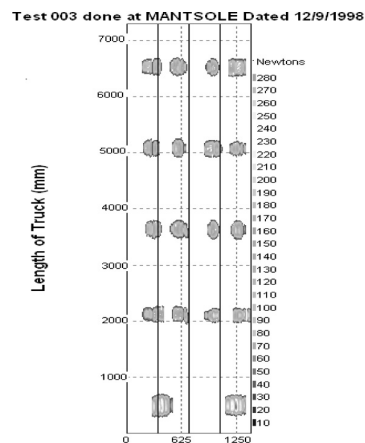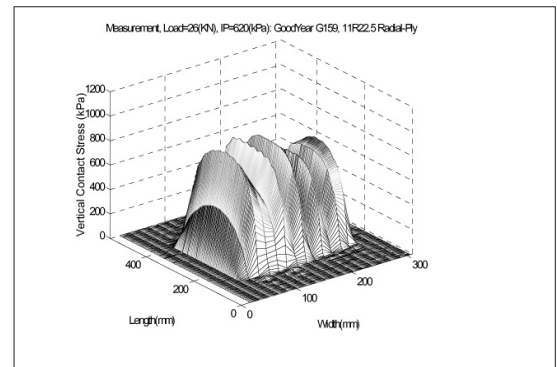
Figure 9
Measured vertical contact stress

Figure 10
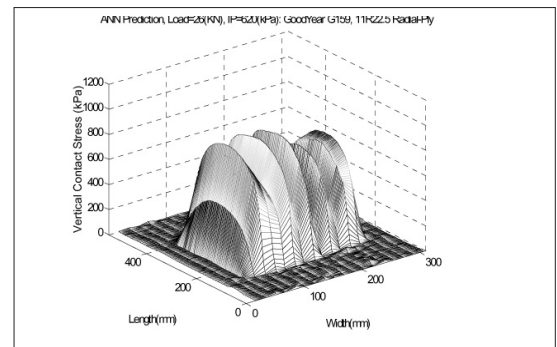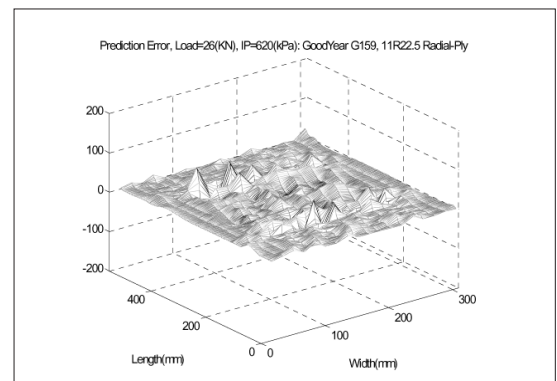ANN prediction: Vertical contact stress

Figure 11
Prediction error: Difference between ANN
prediction and measured vertical contact
stress at a load of 26 kN, and inflation
pressure of 620 kPa.

3.4.2 FEM of a typical new pavement incorporating a thin asphalt surfacing
Layer thickness and material properties
In order to study the effects of non-uniform and non-circular loading (i.e. contact stress) on a typical thinly surfaced
pavement, the NASTRAN code was used for the 3D analysis of the pavement with the layer thicknesses given in
Table 2. The linear elastic material properties used for the analysis are summarised in Table 3. The overall planar
dimensions of the pavement model are a length and width of 3 000 mm with fixed boundaries [Coetzer, 2001].
The mesh consists of eight-noded, sixsided solid elements.

Table 2. Thicknesses of the various layers of the pavement

Layer	Thickness (mm)
Thin Asphalt Surfacing	40
Crushed Stone Base	150
Cementitious Sub-base Upper Layer	150
Cementitious Sub-base Lower Layer	150
Soil Subgrade on Rigid Base	2 000

Table 3. Assumed material properties for the pavement used in the FEM analyses

Layer and temperature conditions	Young's Modulus (E)	Poisson's Ratio (v)	Cohesion (c) (kPa)	Internal Friction Angle (ϕ) degree (°)	Yield Stress (σ_y) (kPa)
for the asphalt layer					
Asphalt Surfacing Cold (< 15 °C)	5 000	0.44	2 000	43	1 462
Asphalt Surfacing Warm (> 20 °C)	1 000	0.44	800	43	585
Asphalt Surfacing Hot (> 40 °C)	200	0.44	160	43	117
Crushed Stone Base	350	0.35	-	-	-
Cementitious Sub-base	1 500	0.35	-	-	-
Soil Subgrade on Rigid Base	100	0.35	-	-	-

For the asphalt material, use was made of a stress-dependent material failure model using a Mohr-Coulomb yield function. All load cases were analysed at three different temperature conditions for the asphalt layer, to simulate seasonal effects. The material properties used here were derived from previous research [Tan et al, 1994].

Loading and Constraints

The tyre loading and inflation pressure cases used for the FEM analyses are summarised in Table 4.

Table 4. The tyre load and inflation pressure cases analysed

LOADING CASES	LOADING VALUES
Load Case 1 (Assumed standard load case (SLC))	Standard uniform circular 20 kN, 520 kPa
Load Case 2 (SIM Measured)	SIM load 26 kN, 420 kPa inflation *
Load Case 3 (SIM Measured)	SIM load 26 kN, 690 kPa inflation
Load Case 4 (SIM Measured)	SIM load 31 kN, 690 kPa inflation

* SIM = Stress-In-Motion (for measured 3D loads)

Load Case 1 was applied as an assumed uniform circular pressure load, while Load Cases 2 to 4 were applied as discrete forces (loads) at the node points based on the measured SIM data (i.e. 3Dloads). The measured SIM load cases used here as load inputs are illustrated in Figures 12 and 13. Load Case 2 shows a typical overloaded/under-inflated case, showing the typical peak stresses at the tyre edges. Load Case 3 is considered representative of normal loading and inflation pressure, and Load Case 4 overloading, with a relative representative inflation pressure. The tyre prints are also given for the three SIM load cases, as shown in the right side of Figure 13. An increase in tyre loading or a decrease in inflation pressure results in an increase in the length of the tyre contact patch, while the tyre width remains constant. For the reduction of the measured SIM loads, the method suggested by Blab [1999] and Blab and Harvey [2000] was used. A separate software program, SIM Analysis.exe, was used [Blab, 1999] to produce the corresponding discrete load input files used for the NASTRAN FEM code in this paper.

Analyses and Results

Full 3D analyses were done with all load cases given in Table 4. The aim of these analyses was to isolate those pavement response parameters that may assist to explain the near surface failures such as rutting (plastic yield) and cracking from the surface downwards. In addition, in order to study the relative contribution of the *separate load components* on pavement response, the 3D SIM Load Case 3 was separated into the X, Y, and Z - load components. Each of these component loads was then applied in the FEM pavement model. The pavement responses of each of these load components were then quantified. The results and summary discussions are given below.

The parameters selected for this study include:
- Vertical Compressive Strain (ε_{zz})
- Maximum Vertical Compressive Stress (σ_{zz});
- Maximum First Invariant of Stress ($I1$);

- Maximum of The second invariant of deviatoric strain ($J'2$ - Strain);
- Maximum second invariant of deviatoric stress ($J'2$ - Stress); and
- Maximum yield values for estimation of Mohr-Coulomb yield failure in the asphalt surfacing.

Both the magnitude and position of the parameters above were determined in the pavement analysed here. These are summarised in Tables 5, 6, 7, 8 and 9. The positions of the x, y and zcoordinate values used in the tables are relative to the centre of the area of the load patch on the surface of the pavement. The z-direction is the same as that used in the finite element analysis and is from the top of the pavement, indicating pavement (or layer) depth.
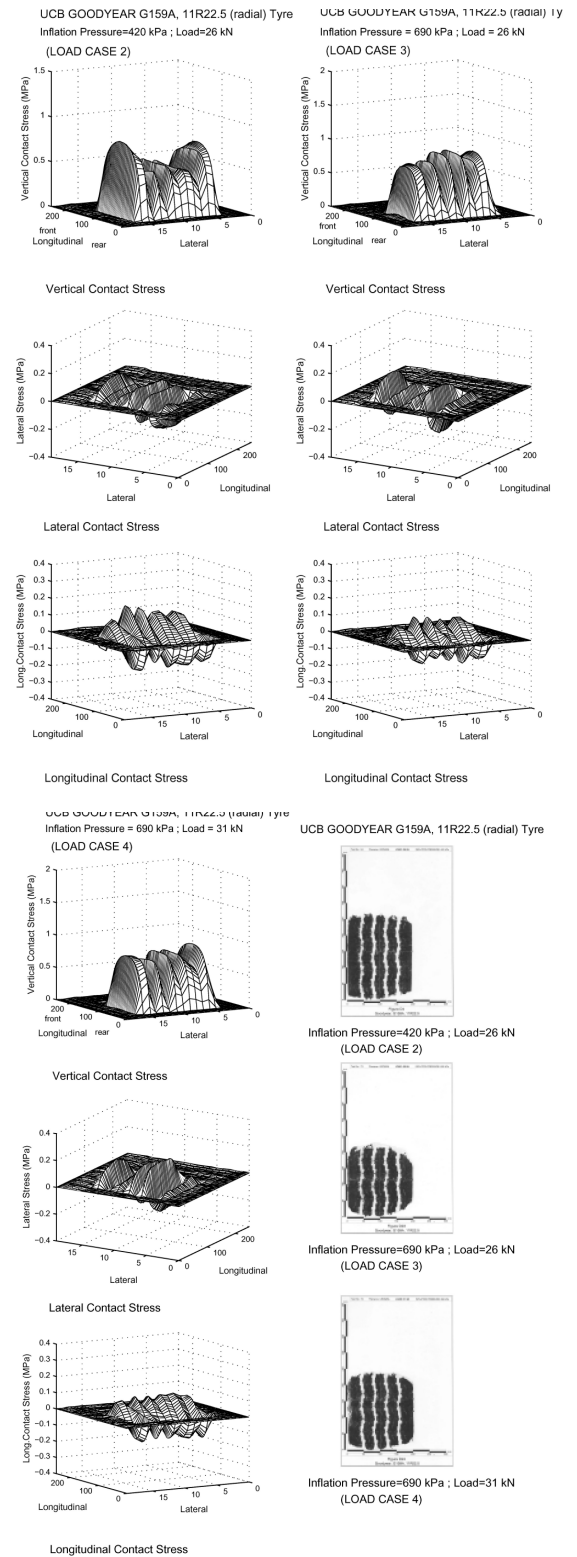
Figure 12
Measured 3D tyre-pavement
contact stresses of Load Cases 2 and 3

Figure 13
Measured 3D tyre-pavement contact stresses
of Load Cases 4, and the associated tyre
prints of Load Cases 2, 3 and 4.

Vertical Compressive Strain (ε_{ZZ})

The calculated maximum vertical elastic compressive strains in the top of the pavement are summarised in Table 5.

Table 5. Maximum calculated compressive strains and their location in the pavement for the four load cases *

Load Case	Strain (µstrain)			x –Position (mm) **			y-Position (mm)			z –Position (mm)		
	Cold	Warm	Hot	Cold	Warm	Hot	Cold	Warm	Hot	Cold	Warm	Hot
1 (SLC)	802	990	1 297	±4.7	±4.7	±61.9	±5.3	±5.3	±78.9	90	90	13.3
2 (SIM)	780	861	2 770	-17.0	-17.00	-17.0	-8.5	-25.5	-17.0	90	90	13.3
3 (SIM)	952	1 117	3 346	-25.5	-25.5	-25.5	-8.5	-8.5	-25.5	90	90	0.0
4 (SIM)	1 030	1 218	2 932	-17.0	-17.0	-34.0	-8.5	-25.5	42.5	90	90	0.0
Load Case 3: Separate Load – Components (Hot case only)												
X-Component	-	444	-	-	-26.5	-	-	8.5	-	-	0.0
Y-Component [6]	-	478	-	-	-9.5	-	-	-42.5	-	-	0.0
Z-Component	-	3 119	-	-	-26.5	-	-	8.5	-	-	0.0

* Note: Compressive as +ve

** Co-ordinates from centre of tyre patch. Note that for cold, warm and hot conditions of the SLC the compressive strains spread almost uniformly over the full area of the applied load, with local maxima on the indicated locations. These co-ordinates are also a function of the fineness of the FEM mesh. For Load Case 1 (SLC), the maximum compressive strains occur at four x, y - symmetrical locations. For the cold and warm conditions of the SLC these locations are near the centre of the load at co-ordinates (4.7,5.3), (-4.7,-5.3), (-4.7,5.3) and (4.7,-5.3).

The strain generally increases with an increase in temperature, although the point at which the maximum occurs decreases in depth. For the cold and warm conditions of Load Cases 1 and 2 the maximum compressive strains occur near the centre of the load, and moves more towards to the edge of the load when asphalt is hot. For Load Cases 3 and 4 the x and y positions of the maximum strain values occur almost at the positions of maximum applied stress, and are also influenced by the temperature. In the cold and warm cases the maximum strain occurs at a point one third of the thickness of the crushed stone base (measured from the top of the layer), and in the hot case this maximum occurs either close to or at the surface of the asphalt. It was also noted that negative strains occur on the asphalt surface between the ribs of the tyre tread pattern, which may be indicative of "dilution" at these positions.

For the X, Y and Z - Component loads (Load Case 3 – Hot condition) these maxima all occur on the surface of the asphalt. The results also indicate that the strain values of the X and Y - Components are approximately 14 and 15 per cent of that of the Z - Component, respectively. The strain value from the Z - Component is approximately 2.5 times the strain value of the standard load case (SLC), while those of the X and Y - Components are only approximately 34 per cent and 37 per cent that of the SLC, respectively.

Vertical Compressive Stress (σ_{ZZ})

The calculated maximum vertical elastic compressive stresses in the top of the pavement are summarised in Table 6. The measured load cases (Cases 2 to 4) produced contact stresses much higher than the normally assumed value of 520 kPa. The maximum vertical compressive stress increases slightly with an increase in temperature, with the maximum occurring on the surface of the asphalt. For the standard load case (Load Case 1) the increase in stress between the hot and cold cases is 3 per cent, while for the measured loads this increase varies between 1 per cent for Load Cases 3 and 4, and 4 per cent for Load Case 2. It is, however, well known that vertical stresses are independent of the elastic moduli in the linear elastic multi theory.

[6] Convergence for the Y - Component load case could not be achieved owing to numerical instabilities in the solution; the values in the tables are those from the last converged solution, which was at 90.5 per cent of the applied load.

Table 6. Maximum calculated vertical compressive stress and its location for the four load cases *

	Load Case Stress (kPa)			x –Position (mm) **			y-Position (mm)			z –Position (mm)		
	Cold	Warm	Hot	Cold	Warm	Hot	Cold	Warm	Hot	Cold	Warm	Hot
1 (SLC)	508	519	521	±42.9	±4.7	±42.9	±89.5	±5.3	±89.5	0.0	0.0	0.0
2 (SIM)	853	869(829)	886	-17.0	-17.0	-17.0	93.5	93.5	93.5	0.0	0.0	0.0
3 (SIM)	1 104	1116(909)	1 113	-25.5	-8.5	-8.5	8.5	8.50	-25.5	0.0	0.0	0.0
4 (SIM)	973	987 (935)	987	-17.0	17.0	17.0	8.5	8.5	8.5	0.0	0.0	0.0
Load Case 3: Separate Load – Components (Hot case only)												
X-Component	-	26		-	-	93.5	-	-	-59.5	-	-	26.7
Y-Component	-	35		-	-	-9.5	-	-	-76.5	-	-	26.7
Z-Component	-	1 136		-	-	-25.0	-	-	8.5	-	-	0.0

* Note: Compressive as +ve

** Co-ordinates from centre of tyre patch. Note that for the SLC the vertical compressive stress spread almost uniformly over the full area of the applied load, with local maxima at the indicated locations. These co-ordinates are also a function of the fineness of the FEM mesh. For Load Case 1, the maximum compressive stress occurs actually at four x, y - symmetrical locations. For the cold and hot conditions of the SLC these locations (local maxima) are near the edge of the load at co-ordinates (42.9, 89.5), (-42.9, 89.5), (-42.9, -89.5) and (42.9, -89.5).

( ) Measured input stresses

Graphical results of the compressive stresses for the four load cases are illustrated in Figures 14, 15, 16 and 17. Note the irregular patterns of compressive stresses under the loaded areas for the SIM measured load cases, compared to the uniform circular pattern in Load Case 1 in Figure 14. For the SLC the maximum stress occurs basically uniformly across the load circle (Figure 14), while for the other load cases the maxima occur away from the tyre centre and closer to the tyre edges, for example in Load Cases 2 and 4. See "darker" areas in Figures 15 and 17. These edge stresses were also clear in the input data, and are typical for overloaded/under-inflated tyres. See Figure 12. This illustrates clearly why it may be more realistic to incorporate actual tyre-pavement loads/stresses for a more rational design of thin (asphalt) surfacings.

For the component loads (Load Case 3 – Hot condition) the maximum stresses occur at a point twothirds of the thickness of the asphalt, measured from the top of the asphalt layer, for the in-plane loads and at the surface of the asphalt for the through-thickness loads. The results indicate further that the values of the X and Y - Components are between 2 and 3 per cent of those of the Z - Component, respectively. The Z - Component is approximately 2.2 times the stress value of the SLC, while the vertical stresses resulting from the X and Y - Components are only approximately 5 and 7 per cent that of the SLC, respectively and occur at a point approximately two thirds of the depth of the asphalt layer, measured from the top of the layer.

Maximum First Invariant of Stress (I_1)

The maximum First Invariant of Stress ($I1$) (also referred to as "bulk stress") was also calculated for the four load cases. The results summarised in Table 7.

The data in Table 7 show clearly that the maximum First Invariant of Stress ($I1$) occurs on the surface of the pavement for all the load cases investigated here. The stress decreases with an increase in temperature, with the maximum occurring on the surface of the asphalt. For the standard load case (Load Case 1) the decrease in the first invariant of stress between the hot and cold cases is approximately 70 per cent, while for the measured loads this decrease varies between 48 per cent for Load Case 2 and 59 per cent for Load Case 4.

Figure 14
Load Case 1: Vertical Compressive Stress in
z-direction (Standard Load Case (SLC):
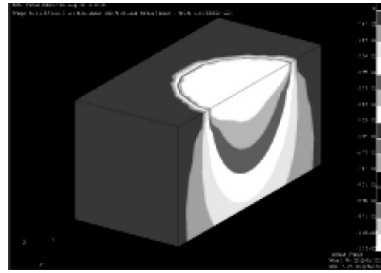circular and uniform)

Figure 15
Load Case 2: Vertical Compressive Stress
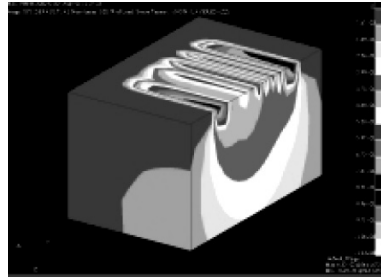in z-direction (Note irregular stress regime)

Figure 16
Load Case 3: Vertical Compressive Stress in
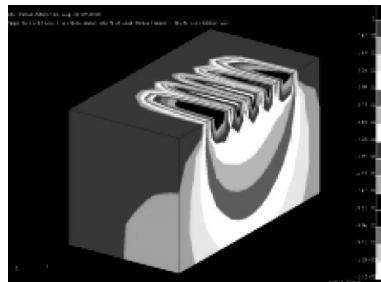z-direction (Note irregular stress regime)

Figure 17
Load Case 4: Vertical Compressive Stress
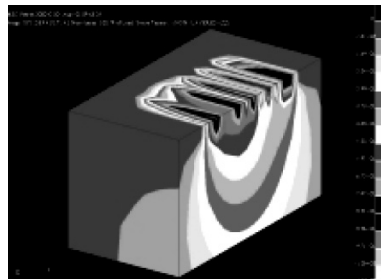in z-direction (Note irregular stress regime

Table 7. Maximum calculated First Invariant of Stress ($I1$) and its location for the load cases *

Load Case	First Invariant of Stress (kPa)			x –Position (mm) **			y-Position (mm)			z –Position (mm)		
	Cold	Warm	Hot	Cold	Warm	Hot	Cold	Warm	Hot	Cold	Warm	Hot
1 (SLC)	4 502	2 046	1 354	±4.8	±4.7	±4.8	±5.3	±5.3	±78.9	0.0	0.0	0.0
2 (SIM)	3 902	2 408	2 016	-68.0	-51.0	-17.0	-76.5	-93.5	93.5	0.0	0.0	0.0
3 (SIM)	5 480	2 886	2 274	-25.5	25.5	-59.5	8.50	8.50	-76.5	0.0	0.0	0.0
4 (SIM)	5 468	2 876	2 239	-17.0	-68.0	-68.0	-25.5	-71.5	-76.5	0.0	0.0	0.0
Load Case 3: Separate Load – Components (Hot case only)												
X-Component	-	242	-	-	-	93.5	-	-	8.5	-	-	0.0
Y-Component	-	287	-	-	-	-25.5	-	-	-76.5	-	-	0.0
Z-Component	-	2 302	-	-	-	-8.5	-	-	8.5	-	-	0.0

* Note: Compressive as +ve

** Co-ordinates from centre of tyre patch. Note that these co-ordinates are also a function of the fineness of the FEM mesh. For Load Case 1, the maximum $I1$ - Stress occurs at four x, y - symmetrical locations. For the cold and warm conditions of the SLC the stress distributuion is bell-shaped, with maxima locations near the centre of the load at (4.8, 5.3), (-4.8, -5.3), (-4.8, 5.3) and (4.8, - 5.3). For the SLC (hot conditions) the I_1 - Stress spread almost uniformly over the full area of the circular load with local maxima close to the edge of the applied circular load patch.

Previous studies indicated that the maximum First Invariant of Stress (*I1*) could effectively be used to describe and quantify the rutting potential as a result of volume change in asphalt materials [Weissman, 1997, Long, 2001]. For the component loads these maxima all occur on the surface of the asphalt. The values of the X and Y - Components are approximately 10 and 12 per cent of that of the Z - Component, respectively. The stress resulting from the Z - Component is approximately 1.7 times the bulk stress value of the SLC, while those resulted from the X and Y - Components are only approximately 18 and 21 per cent that of the SLC, respectively.

Maximum Second Invariant of Deviatoric Strain (*J'₂* - Strain)

The Maximum Second Invariant of Deviatoric Strain (*J'2* - Strain) was also calculated for the four load cases. The results are summarised in Table 8.

Table 8. Maximum calculated Second Invariant of Deviatoric Strain (*J'2* - Strain) and its location for the four load cases *

Load Case	Second Invariant of Deviatoric Strain ($\times 10^{-6}$)			x –Position (mm) **			y-Position (mm)			z –Position (mm)		
	Cold	Warm	Hot	Cold	Warm	Hot	Cold	Warm	Hot	Cold	Warm	Hot
1 (SLC)	0.349	0.539	1.046	±4.8	±4.7	±61.9	±5.3	±5.3	±78.9	90.0	90.0	13.0
2 (SIM)	0.316	0.390	5.360	-17.0	-17.0	-17.0	-25.5	-42.5	93.5	90.0	90.0	13.0
3 (SIM)	0.483	0.674	6.710	-25.5	-25.5	-25.5	-8.50	-8.50	-25.5	90.0	90.0	0.0
4 (SIM)	0.564	0.833	5.159	-17.0	-34.0	-34.0	-8.5	-25.5	42.5	90.0	90.0	0.0
Load Case 3: Separate Load – Components (Hot case only)												
X-Component	-	0.451	-	-	110	-	-	-26.5	-	-	0.0
Y-Component	-	0.712	-	-	-9.5	-	-	-76.5	-	-	0.0
Z-Component	-	6.110	-	-	-25.5	-	-	8.5	-	-	0.0

* Note: Compressive as +ve ** Co-ordinates from centre of tyre patch. Note that these co-ordinates are also a function of the fineness of the FEM mesh. For Load Case 1, the maximum occurs at four x, y - symmetrical locations. For the cold and warm conditions of the SLC these locations are near the centre of the load at (4.8, 5.3), (-4.8, -5.3), (-4.8, 5.3) and (4.8, -5.3). The *J'2* - Strain is in a bell-shaped distribution, with local maxima at the tyre centre. For the SLC (hot conditions) the maximum *J'2* - Strain spread almost uniformly over the full area of the applied circular load patch, with local maxima at the edges.

The maximum Second Invariant of Deviatoric Strain (*J'₂* - Strain) increases with an increase in temperature, although the point at which the maximum occurs decreases in depth. For the cold and warm cases this maximum occurs at a point one third of the thickness of the crushed stone base, measured from the top of the layer, and for the hot case this maximum occurs either close to or at the surface of the asphalt. For the standard load case (Load Case 1) the increase in the second invariant of deviatoric strain between the hot and cold cases is 200 per cent, while for the measured loads this increase varies between 815 per cent for Load Case 4, 1 600 per cent for Load Case 2, and 1 300 per cent for Load Case 3.

For the component loads all these maxima occur at the surface of the asphalt. The values of the X and Y - Components are about 7 and 12 per cent of that of the Z - Component, respectively. The (*J'₂* - strain) value resulting from the Z - Component is approximately 5.8 times that of the SLC and those of the X and Y - Components are approximately 40 and 70 per cent of that of the SLC, respectively. Previous studies indicated that the maximum Second Invariant of Deviatoric Strain (*J'₂* - Strain) could effectively be used to describe and quantify the shear potential at constant volume for asphalt materials [Weissman, 1997, 1999; Long, 2001].

Maximum Second Invariant of Deviatoric Stress (*J'₂* - Stress)

The maximum Second Invariant of Deviatoric Stress (*J'₂* - Stress) was also calculated for the four load cases. The results are summarised in Table 9. The Second Invariant of Deviatoric Stress decreases as the temperature increases, although the point at which the maximum occurs increases in depth for Load Cases 1 and 2. For the SLC, the maximum *J'₂* - stress remains close to the centre of the load, but moves to the edge of the tyre for Load Case 2. For Load Cases 2 the maximum *J'₂* - stress is towards the tyre edges, but for Load Cases 3 and 4 its closer to the tyre

centre, for all temperature conditions investigated here. For Load Case 1 the depth at which the maximum occurs increases from a point on the surface of the asphalt, for the cold case, to a point one third of the way into the crushed stone base, from the top of the base layer, for the hot case. Also for Load Case 2 the depth increases from a point on the surface of the asphalt, for the cold case, to a point one third of the way into the asphalt layer, from the top of that layer, for the hot case. For the SLC the decrease in the second invariant of deviatoric stress between the hot and cold cases is 95 per cent, and for the measured loads this decrease varies between 72 per cent for Load Case 2, 91 per cent for Load Case 4 and 90 per cent for Load Case 3.

Table 9. Maximum calculated Second Invariant of Deviatoric Stress ($J'2$ - Stress) and its location for the four load cases *

Load Case	Second Invariant of Deviatoric Stress			x –Position (mm) **			y-Position (mm)			z –Position (mm)		
	Cold	Warm	Hot	Cold	Warm	Hot	Cold	Warm	Hot	Cold	Warm	Hot
1 (SLC)	0.744	0.054	0.039	±4.8	±23.8	±4.8	±5.3	±15.8	±5.3	0.0	40.0	13.0
2 (SIM)	0.404	0.094	0.114	-51.0	-17.0	-17.0	-76.5	93.5	93.5	0.0	13.3	13.0
3 (SIM)	1.288	0.150	0.131	-25.5	42.5	-25.5	-8.50	-8.50	-25.5	0.0	0.0	0.0
4 (SIM)	1.101	0.118	0.102	-17.0	-102.0	-51.0	25.5	25.5	42.5	0.0	0.0	0.0
Load Case 3: Separate Load – Components (Hot case only)												
X-Component	-	0.011		-	-	-93.5	-	-	-25.5	-	-	0.0
Y-Component	-	0.015		-	-	-8.5	-	-	-76.5	-	-	0.0
Z-Component	-	0.118		-	-	-25.5	-	-	8.5	-	-	0.0

* Note: Compressive as +ve

** Co-ordinates from centre of tyre patch.. Note that for the cold, warm and hot conditions the maximum $J'2$ - Stress occurs in a bellshaped distribution, with local maxima close to the centre of the applied circular load patch. These co-ordinates are also a function of the fineness of the FEM mesh. For Load Case 1, the maximum $J'2$ - Stress occurs at four x, y - symmetrical locations. For the cold conditions of the SLC these locations are near the centre of the load at (4.8, 5.3), (-4.8, -5.3), (-4.8, 5.3) and (4.8, -5.3).

For the other load cases, as well as for the component loads, these maxima occur on the surface of the asphalt. The values of the X and Y - components are approximately 9 and 13 per cent of that of the Z -Component, respectively. The J'_2 - Stress value resulting from the Z - Component only is approximately 3 times the value of the SLC, and those of the X and Y - Components are approximately 28 and 39 per cent of that of the SLC, respectively.

Maximum yield values for estimation of Mohr-Coulomb yield failure in the asphalt surfacing
The yield potentials of all load cases were also calculated. The results are summarised in Table 10.

Table 10. Maximum calculated yield value and its location for the four load cases. The yield potentials (as percentages of plastic yield value) are indicated in brackets.

Load Case	Maximum Yield Criteria (kPa)			x –Position (mm) **			y-Position (mm)			z –Position (mm)		
	Cold	Warm	Hot	Cold	Warm	Hot	Cold	Warm	Hot	Cold	Warm	Hot
1 (SLC)	555	337	267	±4.8	±4.8	±14.3	±5.3	±5.3	±78.9	40.0	13.3	0.0
	(38)	(58)	(228)									
2 (SIM)	461	421	305	-68.0	-34.0	-17.0	-59.5	-93.5	-93.5	40.0	0.0	0.0
	(32)	(72)	(261)									
3 (SIM)	600	522	373	-42.5	8.5	-93.5	-42.5	8.50	-76.5	40.0	0.0	0.0
	(41)	(89)	(319)									
4 (SIM)	710	565	369	-17.0	-17.0	-102	-42.5	-76.5	-76.5	40.0	0.0	0.0
	(49)	(97)	(315)									

Table 10. Maximum calculated yield value and its location for the four load cases. The yield potentials (as percentages of plastic yield value) are indicated in brackets. (Cont.)

Load Case	Maximum Yield Criteria (kPa)			x –Position (mm) **			y-Position (mm)			z –Position (mm)		
	Cold	Warm	Hot	Cold	Warm	Hot	Cold	Warm	Hot	Cold	Warm	HotLoad
Case 3: Separate Load – Components (Hot case only)												
X-Component	-	132		-	-	-8.5	-	-	8.5	-	-	0.0
		(113)										
Y-Component	-	56		-	-	-42.5	-	-	-76.5	-	-	0.0
		(48)										
Z-Component	-	384		-	-	-25.5	-	-	-76.5	-	-	0.0
		(328)										

* Note: Compressive as +ve ** Co-ordinates from centre of tyre patch. Note that for the cold and warm conditions the Yield value occurs in a bell-shaped distribution, with local maxima close to the centre of the applied circular load patch. These co-ordinates are also a function of the fineness of the FEM mesh. For Load Case 1, the maximum Yield values occurs at four x, y - symmetrical locations. For the cold conditions of the SLC these locations are near the centre of the load at (4.8, 5.3), (-4.8, -5.3), (-4.8, 5.3) and (4.8, -5.3). For the hot case the Yield value is uniformly distributed over the circular load patch. **( ) = Percentage of plastic yield value**

For the cold case the absolute maximum calculated values of the yield for all cases occur at the interface between the asphalt and the crushed stone base layers, for all four of the load cases. For the warm and hot cases these values occur either at a point one third of the way through the thickness of the asphalt (Load Case 1, warm) or on the surface of the asphalt, which correlates well with field observations, showing plastic deformation patterns of the tyre tread on the surface of the asphalt in hot conditions.

For the X, Y and Z - Component loads the absolute maxima all occur on the surface of the asphalt. The yield values from the X and Y - Components are approximately 34 and 15 per cent of that of the Z - Component, respectively. The calculated yield value from the Z - Component is approximately 1.5 times the yield value calculated from the SLC, and those of the X and Y - Components are approximately 49 per cent and 21 per cent of that of the SLC, respectively. It is clear that the maximum yield points are mostly localised on top or within the asphalt-surfacing layer, especially when the asphalt layer is "hot". Irregular patterns similar to those produced for the bulk stress were obtained for the yield values. These findings are in line with those of Drakos et al [2001] who recently investigated near-surface rutting under the ribs of radial and bias tyres.

Discussion of FEM results
The results appear to be quite promising and clearly show the localised effects for most of the pavement response parameters studied here by using the realistic (SIM) tyre loads in contrast to the standard uniform circular distributed pressure load. For example, in the hot case the following observations are evident from the actual SIM loads *relative* to the SLC:
- Vertical Strain: 2.1 to 2.6 times higher;
- Vertical Stress: 1.7 to 2.1 times higher;
- Bulk Stress: 1.5 to 1.7 times higher;
- J'_2 - Strain: 5.1 to 6.4 times higher;
- J'_2 - Stress: 2.9 to 6.3 times higher;
- Potential Yield: 1.14 to 1.4 times higher.

For the *separate* X, Y and Z - Component loads, the following relative contributions were found for the SIM loads, *relative* to the SLC (which has vertical circular load only):
- Vertical Strain: X and Y: 34 to 37 per cent, 250 per cent for Z;
- Vertical Stress: X and Y: 5 to 7 per cent, 220 per cent for Z;
- Bulk Stress (*I1*): X and Y: 18 to 21 per cent, 170 per cent for Z;
- J'_2 - Stress: X and Y: 40 to 70 per cent, 580 per cent for Z;
- J'_2 - Stress: X and Y: 28 to 39 per cent, 300 per cent for Z;
- Potential Yield: X and Y: 21 to 49 per cent, 150 per cent for Z.

From the above it is clear that, for most of the response parameters studied here, there are substantial contributions, not only from the measured 3D SIM load application relative to the SLC, but also from the individual X and Y - Component loads. In the case studied here, it appears that, by comparison with those of the SLC, the strain response parameters produced by the 3D SIM loading (or the X, Y - Component loading applications) seem to be more sensitive than perhaps the stress response parameters based on the linear elastic layered theory.

In terms of yield, it is also clear that the lower asphalt moduli (i.e. the "hot" asphalt) case, results in the calculated yield potentials *exceeding* the yield limit for all load cases studied, including the X- load component. *This reinforces the importance of including lateral contact loads/stresses in studies relating to thin asphalt surfacings on pavements, especially in hot climates such as those in southern Africa*.
In the next section additional (more simplified) FEM results *under variable loading and contact stress conditions* on a cracked pavement with a granular base with stress-stiffening material model are discussed.

3.4.3 Effect of varying load and/or contact stress using a custom semi-analytical FEM
In this section, the effects of tyre loading and/or contact stress value on a typical old (cracked) pavement with a thin surfacing are investigated, using a more simplified "Semi-Analytical FEM" approach [Jooste and Kartsounis, 2000]. The purpose of this analysis is to illustrate that the level and shape of contact stress may influence the structural performance of the thin asphalt layer more than perhaps only the tyre load. These FEM analyses were done with a rectangular tyre patch, which is a more improved shape than the traditional circular assumption, especially under overloading/under-inflation conditions (See previous Figure 13, Load Case 2 tyre prints). The length-to-width ratio of the load area can be changed to suit a particular type of tyre or load situation. In this case the tyre width was fixed at 200 mm, which corresponds to actual measurements done on truck tyres (radial and bias ply), under varying load and inflation pressure conditions. In the FEM load model used here, the load length is therefore changed on the basis of the prescribed load level and contact pressure. For this practical analysis, the octahedral shear stress was selected as a pavement response parameter because it is a single parameter, which is invariant of the chosen reference axes and provides a concise indication of the shear distortion at any point within the FEM mesh. The octahedral shear or simple derivatives thereof are *often* used in failure criteria. More specifically, it has been used with success in the evaluation of shear failure in asphalt materials [Ameri-Gaznon et al 1988; Perdomo et al, 1999].

To study the potential behaviour of a new thin asphalt overlay under variable loading and applied stress conditions, a cracked pavement and an uncracked pavement were analysed, as a practical example. The purpose was to evaluate the octahedral shear stress evolution and the strain energy of distortion (SED) [Timoshenko, 1951], at the bottom of the new asphalt overlay, with and without cracks in the old asphalt layer. The pavement was similar to that described in Table 3, but with a thickness of 50 mm for both the old and new asphalt layers. The asphalt layers were modelled using a linear elastic material. In the case of the old asphalt vertical cracks were placed in the asphalt. Vertical cracks where also placed within the cementitious subbase layers. The load was modelled as a rectangle, with the width fixed at 200 mm. It is important to note that, since the width of the tyre contact patch is fixed, a change in the load and or tyre contact stress, results only in a corresponding change in the length of the patch, which was also confirmed with the SIM measurements.

The granular base was modelled as non-linear. The stress-sensitive stiffness model assumed for the granular layer is the "universal soil model" developed by Uzan [1985] and Witczak and Uzan [1988]. The model is described by Equation 1:

$$M_r = k_1 \cdot (\Theta)^{k_2} \cdot (\Gamma_{oct})^{-k} \tag{1}$$

Where M_r = Stress sensitive resilient modulus;
         k_1, k_2, k_3 = Material constants;
         Θ = Bulk stress; and
         Γ_{oct} = Octahedral shear stress.
The negative symbol k_3 ensures a decreasing modulus with increasing shear stress and the positive constant k_2 ensures an increase in stiffness with increasing bulk stress. For the analysis presented here, the material constants assumed for the granular base were as follows: k_1=7000 MPa; k_2=0.9 and k_3 = -0.3. These parameters roughly

agree with those presented by Bonaquist [1992] and Witczak and Uzan [1988] for the same material model and for a dense graded crushed stone base. For the load conditions and pavement type analysed, the assumed material constants result in a base stiffness of approximately 350 MPa to 520 MPa beneath the loaded area. It is interesting to note that a higher stiffness was observed towards the bottom of the granular layer. The granular layer is supported by a 300 mm thick high-stiffness cementitious subbase layer with an elastic modulus = 3000 MPa. This increased stiffness of resilient moduli may explain the very good performance of this type of "inverted" granular base pavement structures in South Africa. For comparison purposes, as well as for "benchmarking", the pavement was also modelled using linear elastic analysis with circular loading. The properties of the pavement studied here are given in Table 11 below.

Table 11. Properties of the equivalent pavement used in the benchmarking analysis

Layer	E-Moduli	Poisson's Ratio	Thickness
	(MPa)	(ν)	(mm)
New asphalt (new AC)	2500	0.4	50
Old asphalt (old AC)	3000	0.4	50
Granular Base	450	0.4	150
Cemented Subbase	1800	0.4	300
Subgrade	100	0.4	2000

Note that the FEM uses a rectangular (or square) loading patch, whereas the layered solution assumes a circular load. For the "benchmarking" here, it was decided to compare the elastic surface deflection and the Strain Energy of Distortion (SED). The deflection results are shown in Figure 18, and it is clear that the deflection basin results of the FEM and layered theory solution correspond almost exactly in this case. In Figure 19 the SED at the bottom of the top asphalt layer (44 mm depth) is illustrated. The results indicate the same basic pattern, but different peak values. This result is caused by the *shape* of the load patch, resulting in the *lower* SED for the rectangular FEM load. In Figure 20 and 21 the SED at depths of 137.6 and 457 mm is shown. The results indicate a *relatively good* comparison between the fully analytical linear elastic layered theory and the semianalytical FEM in the *centre region* of the loading, but they deviate as one moves further away from the centre of the loading (Figures 19 and 21). These deviations are directly related to the shape of the load, since a uniform contact stress was assumed here for both cases.

FEM analysis on uncracked and cracked pavement

After the "benchmarking", FEM analyses were done on the *uncracked* and *cracked* pavements. The aim was to evaluate the effects of contact stress level and tyre loading on potential distress such as the traffic-associated reflective cracking potential of a new asphalt overlay. This was done by means of the octahedral shear stresses developed and the SED in this layer, in positions near the cracking in the old asphalt layer. The uniform rectangular load and uniform contact stress cases evaluated here are summarised in Table 12. Note: The SIM 3D loading was *not* used in the FEM analyses in this section.

Table 12. Load cases evaluated with semi-analytical FEM on rehabilitated pavement

Case Dual	Wheel Load[2] (kN)	Contact Stress (kPa)
		[rectangular patch]
1 (Cracked and uncracked)	40	520
2 (Cracked and uncracked)	40	900
3 (Cracked and uncracked)	70	900

[2] Dual wheel load was modelled as a rectangular (i.e. square) patch with fixed width at 200 mm.

Figure 22 shows the octahedral shear stress and strain energy of distortion (SED) iso-lines at different offsets along the centreline of the load axis for the *uncracked* Case 1 (40 kN dual load at 520 kPa contact stress). It can be seen that the octahedral shear stress and SED peak along the edges of the load. This shear effect can also be observed

in a layered elastic analysis and is primarily caused by the high torsion stress that exists in the X-Y plane, and at positions close to the edge of the load. At these positions, the "tipping" or torsion effect is relatively large, exceeding some of the normal stresses. Figure 23 shows the octahedral shear stress and SED lines for the *cracked* case, where the asphalt overlay was placed over a layer with closely spaced cracks. The crack tip "stress effect" is clearly visible, with an increase of over 100 per cent in both the maximum octahedral shear stress and SED. Figure 24 shows the octahedral shear stress and SED for the *uncracked* Case 3 (70 kN dual wheel at 900 kPa contact stress), and Figure 25 for the *cracked* Case 3. The maximum stresses and SED for all cases were evaluated, and the results are given in Figure 26 (octahedral shear stress) and Figure 27 (SED). It is clear that, in both cases, the cracked pavements resulted in the higher (i.e. peak) response defined by the octahedral shear stress, and SED. Further, it is interesting to note that the increase in wheel load from 40 kN to 70 kN, at 900 kPa, does *not* result in a higher shear stress or SED, by comparison with the standard 40 kN load case. This can most likely be attributed to the smaller load area, which causes a higher "punching" effect at shallow depths. The high contact stresses with the standard 40 kN wheel load lead to a relatively short load patch length. This results in a "punching" effect that causes a significant increase in both the octahedral shear stress and SED along the bottom of the new thin asphalt overlay. The increase in both response parameters as a result of an *increase in contact stress* is clearly visible in Figures 26 and 27.

Therefore, considering and evaluating thin asphalt surfacings on cracked pavements, the importance of the potential detrimental effect of increased tyre-pavement contact stresses and a change in load shape from circular to rectangular, should not be under estimated in practice.

4. CONCLUSIONS AND RECOMMENDATIONS
4.1. Conclusions
From the results presented in this paper it is concluded that the incorporation of non-uniform *tyrepavement* contact stresses into pavement design and analysis provide for a much more *rational* understanding of the *tyre-pavement* contact problem. The use of measured contact stresses far better simulate

tyre-pavement loading than the traditional circular shape with uniform loading. It is specifically concluded that:
- The modelled response of the pavement, especially of the upper layers, such as the thin asphalt surfacing, reflects the shape and distribution of the applied (measured) contact stress from tyres more realistically and accurately;
- Pavement response parameters, such as stress or strain, and its invariants, reflect a sensitivity to the shape and distribution of the loading and contact stress near the surface of thin asphalt pavements - especially in "hot" climates;
- The strain response parameters seem to be slightly more sensitive to the loading and material conditions, than the stress parameters. This suggests that these strain parameters might be more suitable candidates for the evaluation of pavement response to elastic deformation, than perhaps the stress parameters;
- For the rehabilitation of cracked pavements the semi-analytical FEM analyses indicated that the potential of reflective cracking from old cracked pavements could be effectively studied.
- The use of octahedral shear stress and strain energy of distortion at the position of cracks reflects the crack potential within the new thin asphalt overlay quite well.
- The investigation also showed that the effect of load shape is equally as important as the load distribution. The rectangular and more realistic load resulted in shear stress and energy patterns different from the traditionally assumed circular pattern.
- Since the measurement of tyre-pavement contact stresses is quite a difficult task, the use and further development of Artificial Neural Networks could greatly assist in predicting the 3D-stresses for load and inflation cases that are not necessarily measured.
- Because of the large quantity of measured contact stress data discussed here, it is of utmost importance to manage *tyre-pavement* contact stresses in an appropriate way, such as by use of the data base approach suggested here.

Figure 18
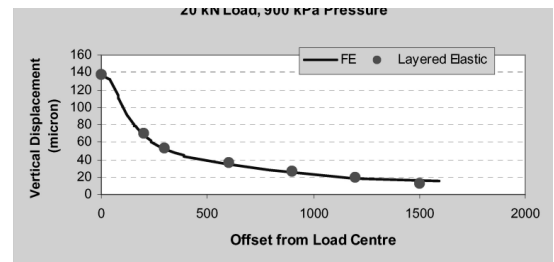Comparison of deflection by
layered elastic and FE method study

Figure 19
SED at bottom (Depth: 44.36 mm) of
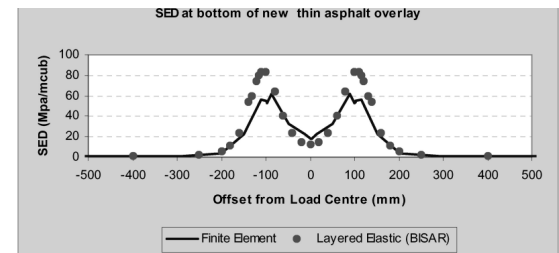the new 50 mm thin asphalt overlay

Figure 20
SED at top part (Depth: 137.6 mm)
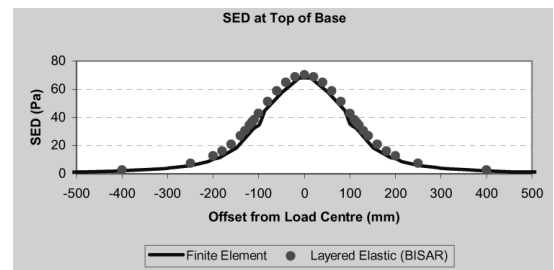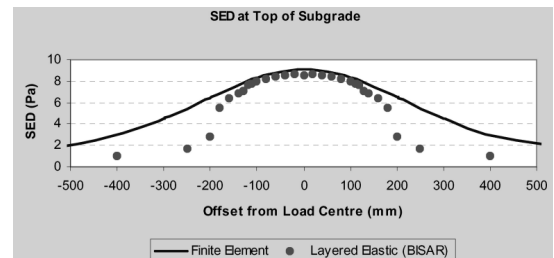of the granular base layer

Figure 21
SED at top part (Depth: 457 mm)
of the subgrade

Integration of the 3D-tyre-pavement contact stress information with mechanistic-empirical pavement design and analysis should be done holistically. The influence of dynamic tyre loading should also be incorporated. In this way, more rational pavement design and analysis will be possible and consequently, despite ever-increasing costs, even more economical thin asphalt pavements could be constructed.

4.2. Recommendations
The following recommendations follow naturally from the work presented here:
- More rational use should be made of measured *3D-tyre-pavement* contact stresses in the design and analysis of flexible pavements, including appropriate material and tyre models;
- Quantification of the effects of lateral loading (X, Y) on the surface of flexible pavements, especially in hot climates, as well as at pavement curves and intersections, should be improved;
- The influence of vehicle (or tyre) speed and tyre type on the 3-dimensional contact patch stress regime on the surface of flexible pavements should be studied;
- Appropriate mechanistic-empirical pavement response parameters for the practical application during the design of thin asphalt layers against rutting and cracking potentials should be isolated;
- Tyre-pavement contact stress data for different types of tyres, loading levels and inflation pressures should be managed in a well organised database for further data validation and post-processing, such as the Artificial

Neural Network approach;

- Appropriate mechanistic-empirical transfer functions between tyre loading/stresses regimes and pavement surface failure should be developed; and
- Laboratory test methods should be calibrated with actual applied tyre-pavement contact stress ranges in order to quantify possible shift factors between laboratory and field more accurately.

5. ACKNOWLEDGEMENTS

6. KEYWORDS

Tyre, pavement, contact stresses, modelling, materials, Finite Element Methods (FEM), thin asphalt, non-uniform.

Figure 22
Octahedral Shear Stress and SED at the bottom of the new thin asphalt overlay, on the *uncracked* asphalt layer under a rectangular loading of 40 kN and 520 kPa
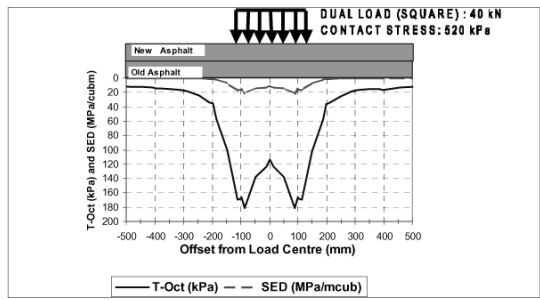
Figure 23.
Octahedral Shear Stress and SED at the bottom of the new thin asphalt overlay, on the *cracked* asphalt layer under a square loading of 40 kN and 520 kPa
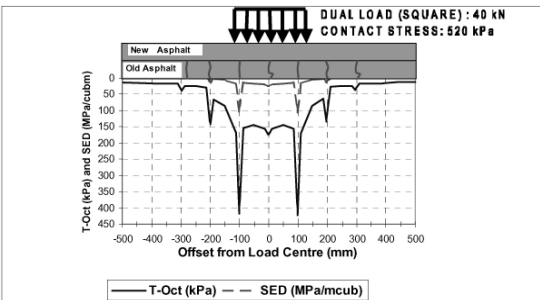

Figure 24
Octahedral Shear Stress and SED at the bottom of the new thin asphalt overlay, on the *uncracked* asphalt layer under a square loading of 70 kN and 900 kPa
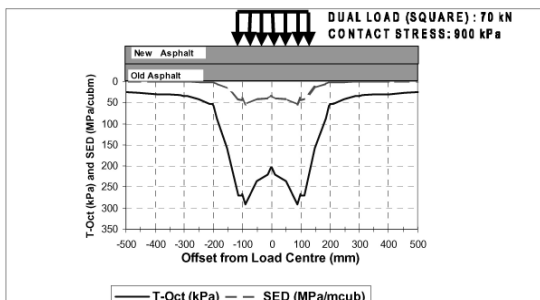
Figure 25
Octahedral Shear Stress and SED at
the bottom of the new thin asphalt
overlay, on the *cracked* asphalt layer
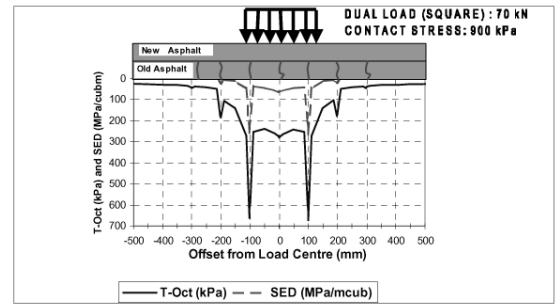under a square loading of 70 kN and
900 kPa

Figure 26
Octahedral shear stress: bottom
of the new thin asphalt layer, under the
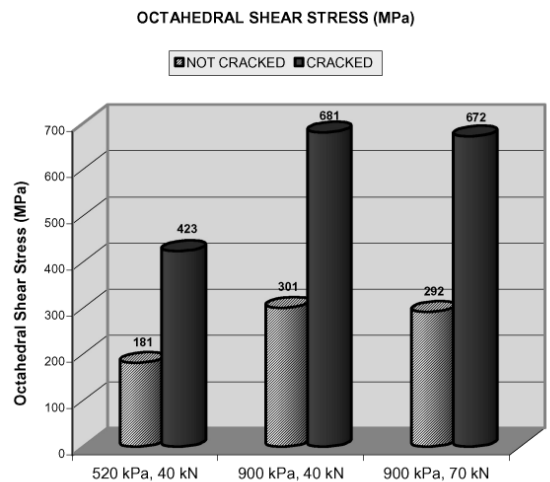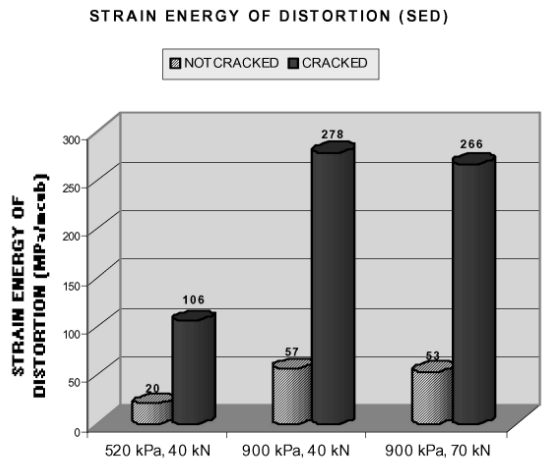various loading conditions

Figure 27
Strain Energy of Distortion (SED): bottom
of the new thin asphalt layer, under the
various loading conditions

7. REFERENCES

Ameri-Gaznon, N, & Little, D N, 1988, Permanent deformation
Potential in Asphalt Concrete Overlays over Portland Cement Concrete
Pavements. FHWA Report No. FHWA/TX-88/452-3F, Austin, Texas,
USA, 1988.

Blab, R, & Harvey, J, 2000, Modelling Measured 3D Tire Contact
Stresses In A Visco-Elastic FE Pavement Model. First National
Symposium on 3D Finite Element Modelling for Pavement Analysis &
Design. Nov 8-10, 1998, Embassy Suites Hotel, Charleston, West
Virginia, USA.

Blab, R, 1999, Introducing Improved Loading Assumptions into
Analytical Pavement Models Based on Measured Contact Stresses of
Tires. International Conference on Accelerated Pavement Testing,
Reno, Nevada, USA, 1999. Paper Number: CS5-3.

Bonaquist, R, 1992, Assessing the Non-linear Behaviour of Subgrades
and Granular Bases from Surface Deflections. Proceedings of the 7th
International Conference on Asphalt Pavements. Volume 2.
Performance. University of Nottingham, Nottingham, UK, August
1992. pp16-31.

Brosseaud, Y, 1999, Very thin and ultra-thin wearing courses using hot-mixed bituminous materials: A review of use and performance. Session N° 270 Effectiveness of a Pavement Preventive Maintenance Program Paper N° 990987. 78th Annual Meeting, in January 1999, *Transportation Research Board*, Washington, D.C., USA.

DADS, 1997, Dynamic analysis and design system. User's guide. Revision 8.5.

Das, B M, (1997). *Advanced Soil Mechanics*, Second Edition, Taylor and Francis, 1997.

Drakos, C, Roque, R, & Birgisson, B, 2001, Effect Of Measured Tire Contact Stresses On Near-Surface Rutting. 80thth Annual Meeting in January 2001, *Transportation Research Board*, Washington, D.C., USA.

De Beer, M, Fisher, C, & Jooste, F J, 1997, Determination of pneumatic tyre-pavement interface contact stresses under moving loads and some effects on pavements with thin asphalt surfacing layers. Proceedings of the Eighth International Conference on Asphalt Pavements (ICAP '97), August 10- 14, 1997, University of Washington, Seattle, Washington, USA. pp179-227.

De Beer, M, 1998a, Development of the Vehicle - Road Surface Pressure Transducer Array Mark III Stress - In - Motion (SIM) system (VRSPTA Mark III SIM): Contract Report CR-98/047, CSIR Transportek, Pretoria, South Africa, November 1998.

De Beer, M, 1998b, Mechanistic Evaluation of the Effects of Increased Uniform Tyre/Pavement Contact Stresses and Axle Loads on the Catalogue Pavement Structures of Draft TRH 4 (1996). Draft External Contract Report CR-98/015, Department of Transport (DoT), Pretoria, South Africa, March 1998.

De Beer, M, Kannemeyer, L, & Fisher, C, 1999, Towards Improved Mechanistic Design Of Thin Asphalt Layer Surfacings Based On Actual Tyre/Pavement Contact Stress - In - Motion (SIM) Data In South Africa. 7th Conference On Asphalt Pavements For Southern Africa (CAPSA '99), Victoria Falls, Zimbabwe, Oct 1999.

De Beer, M, & Fisher C, 2000, Contact Stresses of the 11.00 – R22.5 pneumatic radial tires on the Gautrans Heavy Vehicle Simulator (HVS) measured with the Vehicle-Road Pressure Transducer Array (VRSPTA) system. Confidential Contract Report CR-99/012, March 2000, CSIR Transportek, Pretoria, South Africa, March 2000.

Douglas, R A, Woodward, W D H, & Woodside, A R, 2001, Road Contact Normal and Shear Stresses under Tyres with Low Inflation Pressure. Proceedings of the 20th Australian Road Research Board (ARRB) Transport Research Conference: Managing your road assets, Melbourne Convention Centre, 19-21 March 2001, Melbourne, Australia.

El-Gindy, M, Lewis, H L, & Lewis, A S, 2000, Tire/Pavement Contact-Stress Model Based on an Artificial Neural Network, presented Tuesday, July 20, at the second annual Pennsylvania Transportation Conference at the University. Pennsylvania State University, University Park, Pennsylvania, USA.

Himeno, K, & Ikeda, T, 1997, Distribution of tire pavement contact pressure of vehicles and its influence on pavement distress. Eighth International Conference on Asphalt Pavements (ICAP '97), August 10-14, 1997, Seattle, Washington, USA. pp. 129-139.

HMA, 1998, HMA Project Management Group (PMG) - Business Plan for the HMA Programme, Version 1.1, February 1998, Contact Person: Mr B M J A Verhaeghe, Transportek, CSIR, P O Box 395, Pretoria, 0001, South Africa.

HMA, 2000, Interim Design Guidelines for the Design of Hot-Mix Asphalt in South Africa, Asphalt Academy, CSIR, Pretoria, South Africa, June 2000.

HMA, 2001, Interim Design Guidelines for the Design of Hot-Mix Asphalt in South Africa, Asphalt Academy, CSIR, Pretoria, June 2001.

ISAP, 1997, International Society of Asphalt Pavements. Eighth International Conference on Asphalt Pavements (ICAP '97), August 10-14, 1997, University of Washington, Seattle, Washington, USA.

ISO (1995). International Organisation for Standardisation. Mechanical Vibration – Road surface profiles – reporting of measured data. Genève: ISO. (ISO 8608:1995(E)).

Jooste, F J, & Lourens, J P, 1998. Appropriate models for estimating stresses and strains in asphalt layers. Contract Report CR-98/060, Hot Mix Asphalt Project task: TFA5/A/1. Division of Roads and Transport Technology, CSIR, Pretoria, South Africa, September 1998.

Jooste, F J, & Kartsounis, M, 2000, Cracking In Asphalt Layers: It Influence On Overlay Or Inlay Design. Proceedings of the 4th Malaysian Road Conference, 30-31st October to 1 Nov 2000. Paper 2-5. Kuala Lumpur.

Long, F M, 2001, Permanent Deformation of Asphalt Concrete Pavements: A Non-Linear Visco-Elastic Approach to Mix Analysis and Design. A dissertation submitted in partial satisfaction of the requirements for the degree of Doctor of Philosophy in Engineering-Civil and Environmental Engineering, University of California, Berkeley, California, USA.

MATLAB, 2001, Neural Network Toolbox for use with MATLAB, User Guide Version 4, 2000.

Myers, L A, Ruth, B E, & Drakos, C, 1999, Measurement of Contact stresses for different truck tire types to evaluate their influence on near-surface cracking and rutting. 78th Annual Meeting in January 1999, *Transportation Research Board*, Washington, D.C., USA.

NASTRAN, 2001, MSC. Nastran 2001 & MSC. Patran 2000 Release 2. MSC and MSC. are registered trademarks and service marks of MSC. Software Corporation. NASTRAN is a registered trademark of the National Aeronautics and Space Administration. MSC. Nastran is an enhanced proprietary version developed and maintained by MSC. Software Corporation. MSC. Patran is a trademark of MSC. Software Corporation.

Owen, J, & Hinton, E, 1980, Finite Elements in Plasticity: Theory and Practice. Dept of Civ. Eng, University College of Swansea, UK, Pineridge Press Ltd., 91 West Cross Lane, West Cross, Swansea, UK.

Perdomo, D, & Button, J W, 1991, Identifying and Correcting Rut Susceptible Asphalt Mixtures. Research Report 1121-2F, Texas Transportation Institute, College Station, Texas, USA, 1991.

Ringwood, B, 2001, Personal communications during development of SIM database.

Roque, R, Myers, L A, & Ruth, B E, 1998, Loading characteristics of modern truck tires and their effects on surface cracking of asphalt pavements. Proceedings of the Fifth International Conference on the Bearing Capacity of Roads and Airfields BCRA '98, Volume 1, Trondheim, Norway, 6 to 8 July 1998, pp 93-102.

Steyn, W van der Merwe, 2001, Considerations of Vehicle-Pavement Interaction for Pavement Design. A thesis submitted in partial fulfillment of the requirements for the degree of Philosophiae Doctor (Transportation Engineering) In The Faculty Of Engineering, Built Environment And Information Technology, University of Pretoria, Pretoria, South Africa, January 2001.

Tan, S A, Low, B H, & Fwa, T F, 1994, Behaviour Of Asphalt Concrete Mixtures In Triaxial Compression. Journal of Testing and Evaluation, JTEVA, Vol. 22, No. 3, May 1994, pp. 195-203.

Theyse, H L, De Beer, M, & Rust, F C, 1996, Overview of the South African Mechanistic Pavement Design Analysis Method. Paper Number 96-1294 presented at the 75th Annual Transportation Research Board Meeting, January 7 - 11, 1996, Washington, D.C., USA.

Timoshenko, S, Goodier, J N, 1951, *Theory of Elasticity*, Second Edition, McGRAW-HILL BOOK COMPANY, Inc. New York.

TRH 4, 1996, Structural Design of flexible pavements for interurban and rural roads. Pretoria: Committee of Land Transport Officials (COLTO), Department of Transport (DoT). (DoT Technical Recommendations for Highways; Draft TRH 4 (1996)), Pretoria, South Africa, 1996.

TRH 14, 1985, Guidelines for Road Construction Materials, Department of Transport, Pretoria, South Africa, 1985.

Uzan, J, 1985, Characterization of Granular Material. Transportation Research Record 1022. Washington D.C.: Transportation Research Board (TRR 1022);

Weissman, S L, 1997, The Mechanics of Permanent Deformation in Asphalt-Aggregate Mixtures: A Guide to Laboratory Test Selection**.** Project funded by Federal Highway Administration under contract number M2380 through the Pavement Research Centre Institute of Transportation Studies, University of California, Berkeley, California, USA.

Weissman, S L. 1999. The Influence of Tire-Pavement Contact Stress Distribution on the Development of Distress Mechanisms in Pavements. 78th Annual Meeting in January 1999, Transportation Research Board, Washington, D.C., USA.

Witczak, M, & Uzan, J, 1988, The Universal Airport Design System: Report I, Granular Material Characterization, The University of Maryland, College Park, Maryland, USA, September 1988.

Woodside, A R, 1992, Assessment of the Interfacial Stresses in a Composite Highway Surfacing under Heavy Goods Vehicle Loading. In: *Heavy Vehicles and Roads: Technology, Safety And Policy;* Edited by D. Cebon and C.G.B. Mitchell. (Proceedings of the Third International Symposium on Heavy Vehicle Weights and Dimensions, organised by the University of Cambridge and held at Queen's College, Cambridge, UK, 28 June - 2 July 1992), pp 51 - 58.

Woodside, A R, Wilson, J, & Xin Liu, G, 1992, The Distribution of Stresses at the Interface between Tyre and Road and their Effect on Surface Chippings. Proceedings of the 7th International Conference on Asphalt Pavements. Volume 3. Design and Performance. University of Nottingham, Nottingham, UK, August1992, pp428-442.

Woodside, A R, Woodward W D H, & and Siegfried (1999). The Determination of Dynamic Contact Stress. International Conference on Accelerated Pavement Testing, Reno, Nevada, USA, 1999. Paper Number CS5-2.